S1 BSE and CL images of analyzed crystals and SIMS analysis craters

Numbers refer to the corresponding analyses as indicated in the SIMS data table (red = excluded from weighted mean calculations). Frames and numbers in blue indicate crystals selected for ID-TIMS analysis.

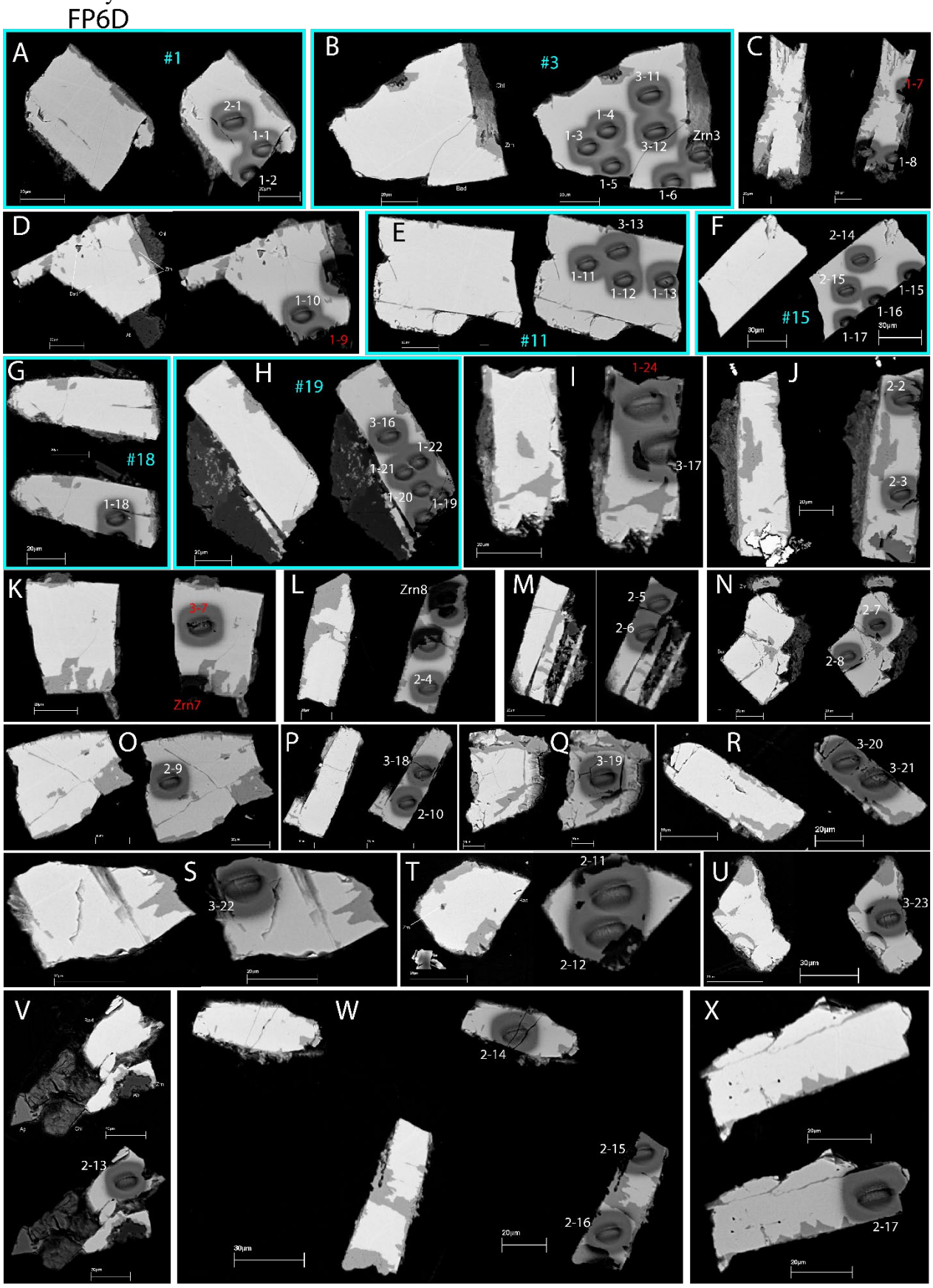

Figure S1. BSE images of analyzed baddeleyite and zircon crystals and SIMS analysis craters of sample FP6D (grain mount).

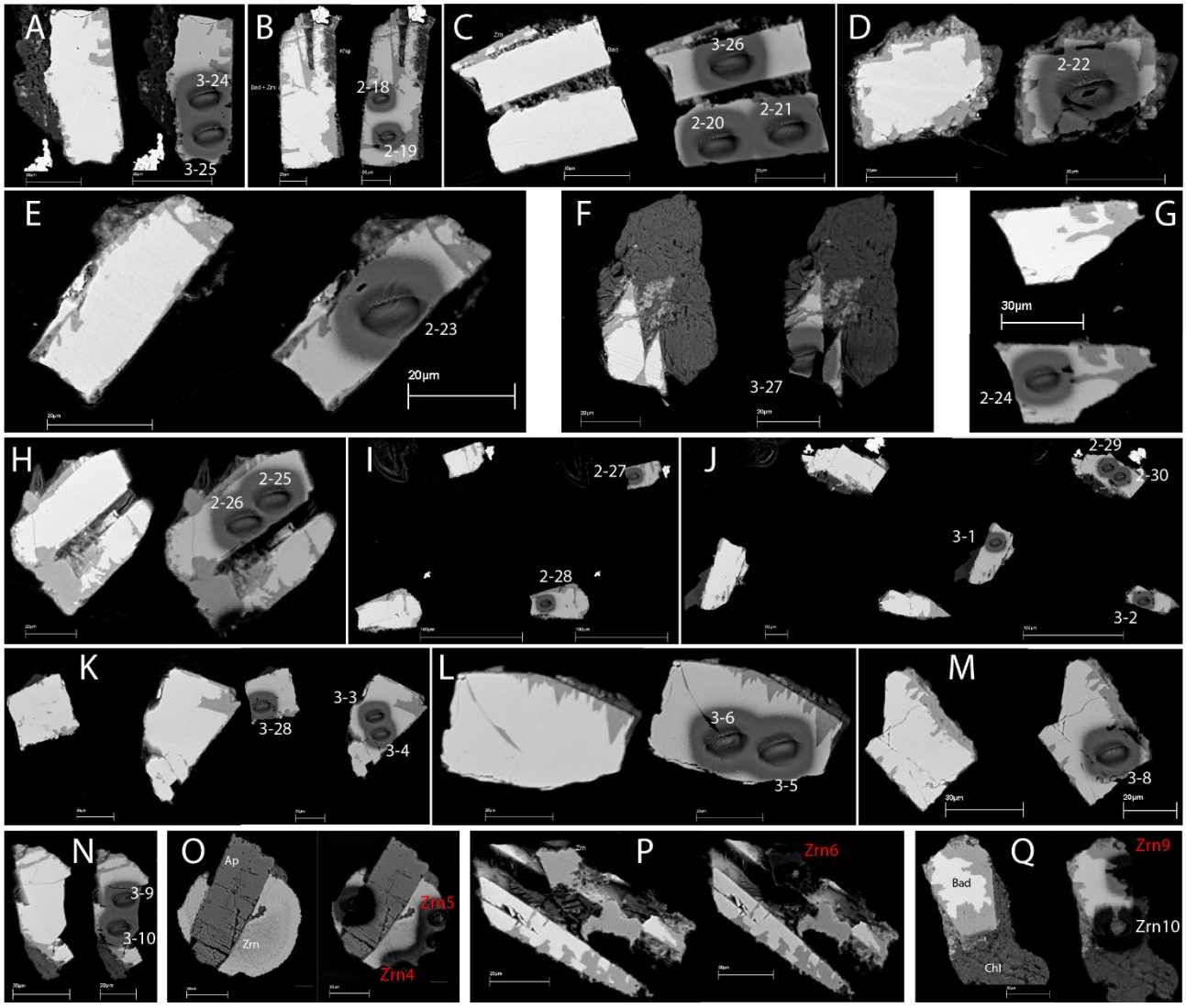

Figure S2. BSE images of analyzed baddeleyite and zircon crystals and SIMS analysis craters of sample FP6D (grain mount), continued.

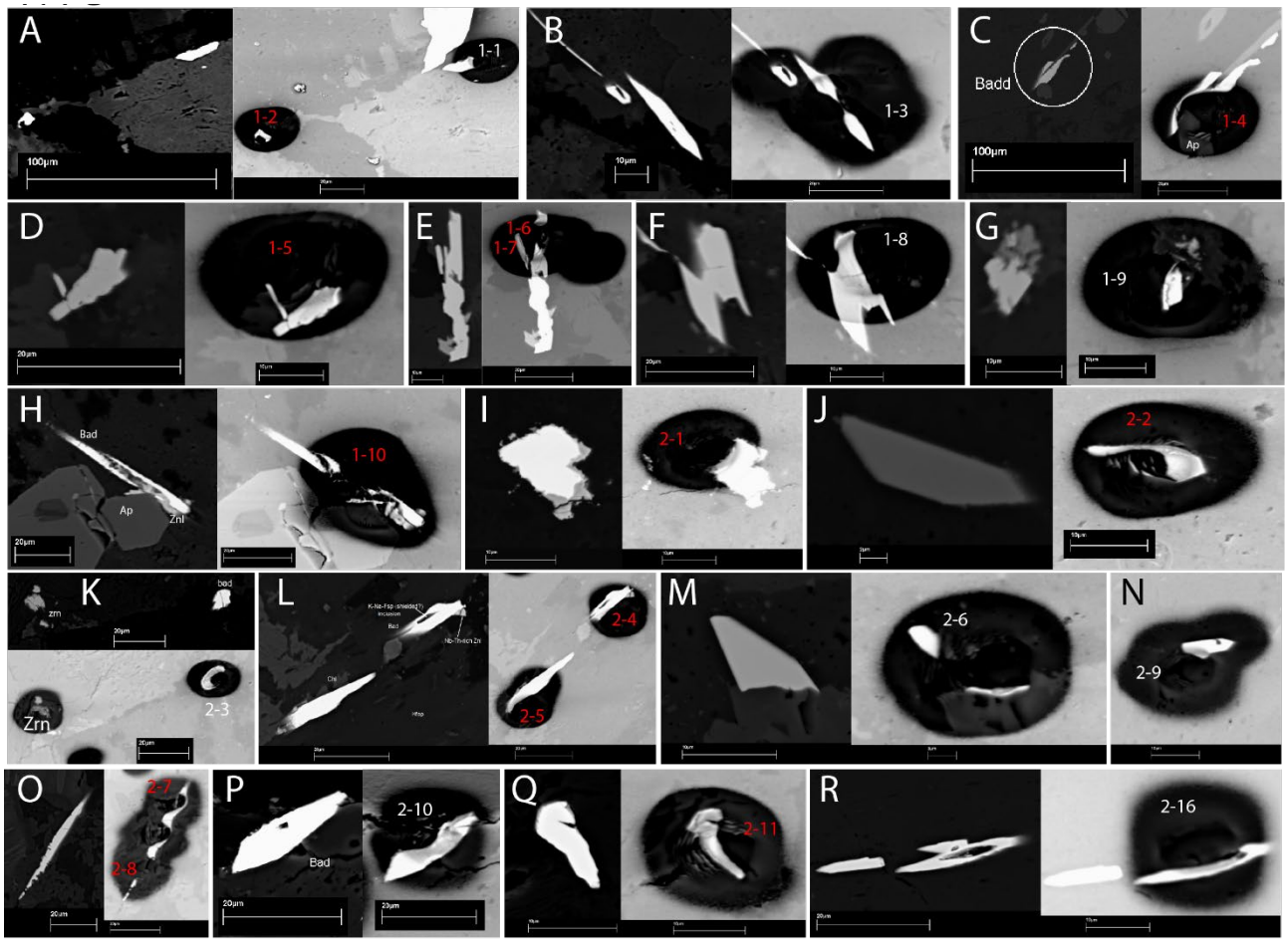

Fig. S3. BSE images of analyzed crystals and SIMS analysis craters of sample FP7G (in situ).

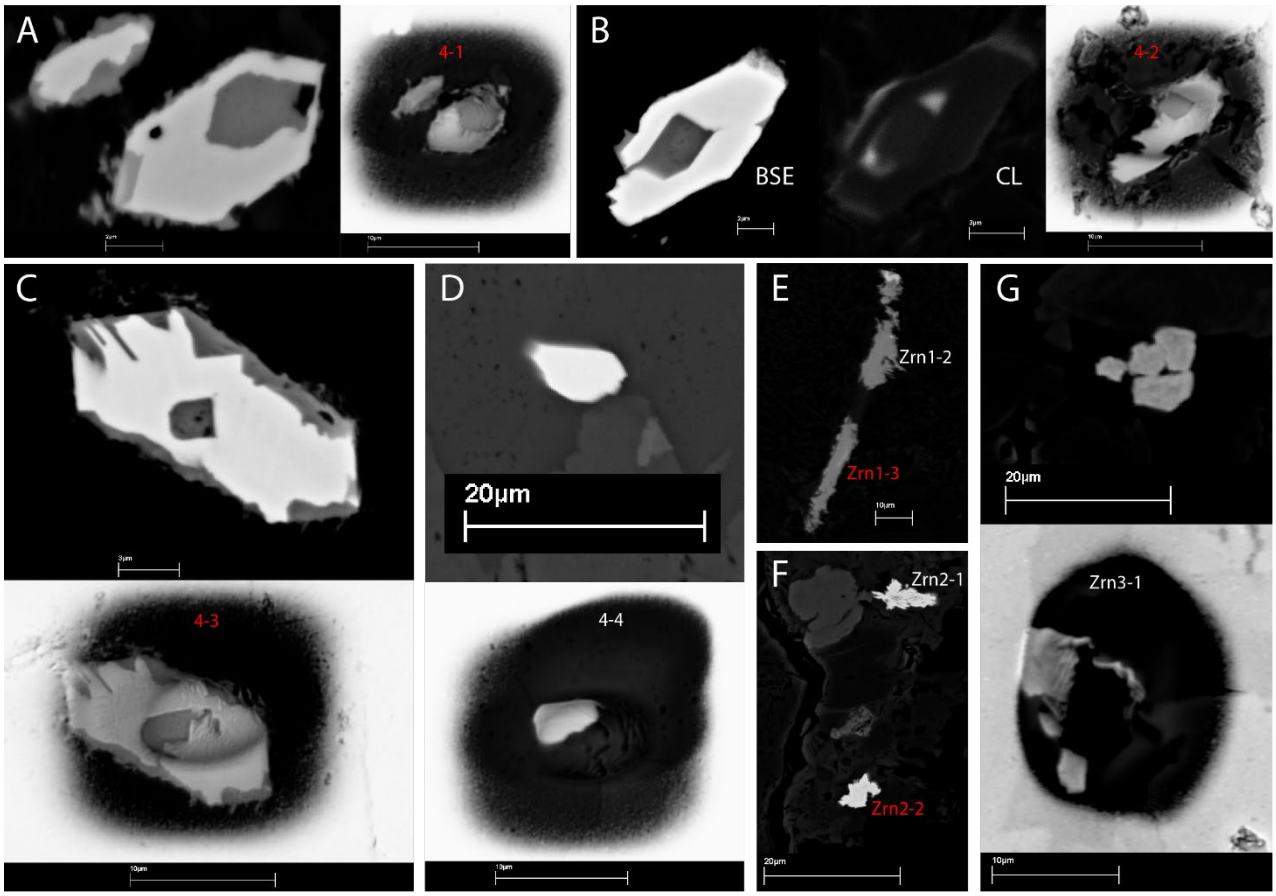

Figure S4. BSE images of analyzed baddeleyite crystals with zircon inclusions and SIMS analysis craters of sample FP12A (in situ).

FP12A

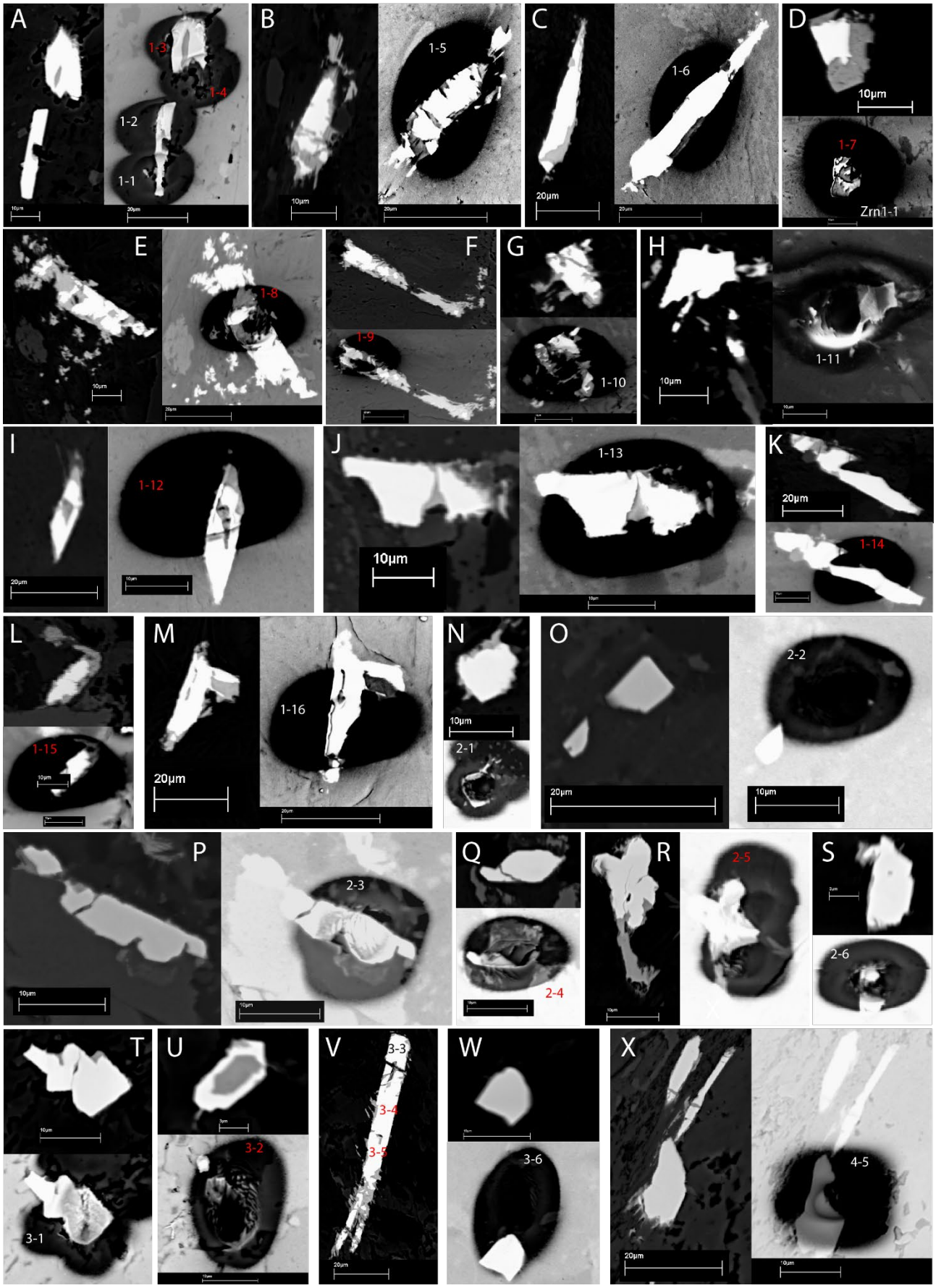

Figure S5. BSE images of analyzed crystals and SIMS analysis craters of sample FP12A (in situ). Numbers refer to the corresponding analyses as indicated in the data table.

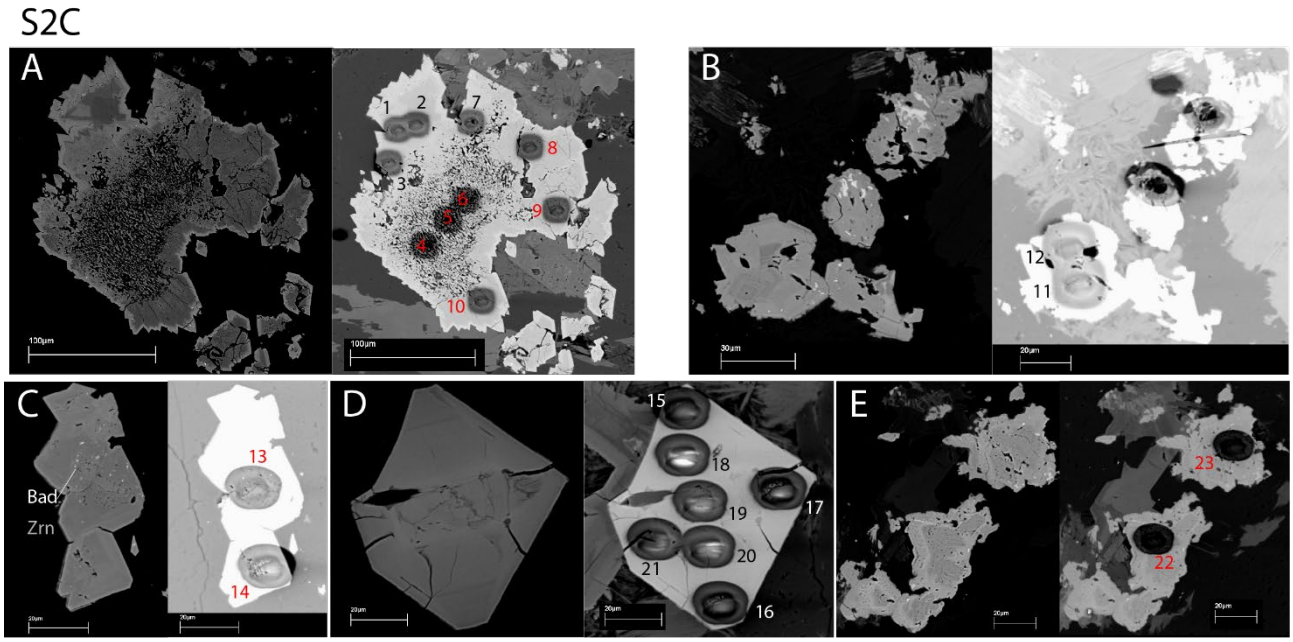

Figure S6. BSE images of analyzed crystals and SIMS analysis craters of sample S2C (in situ).

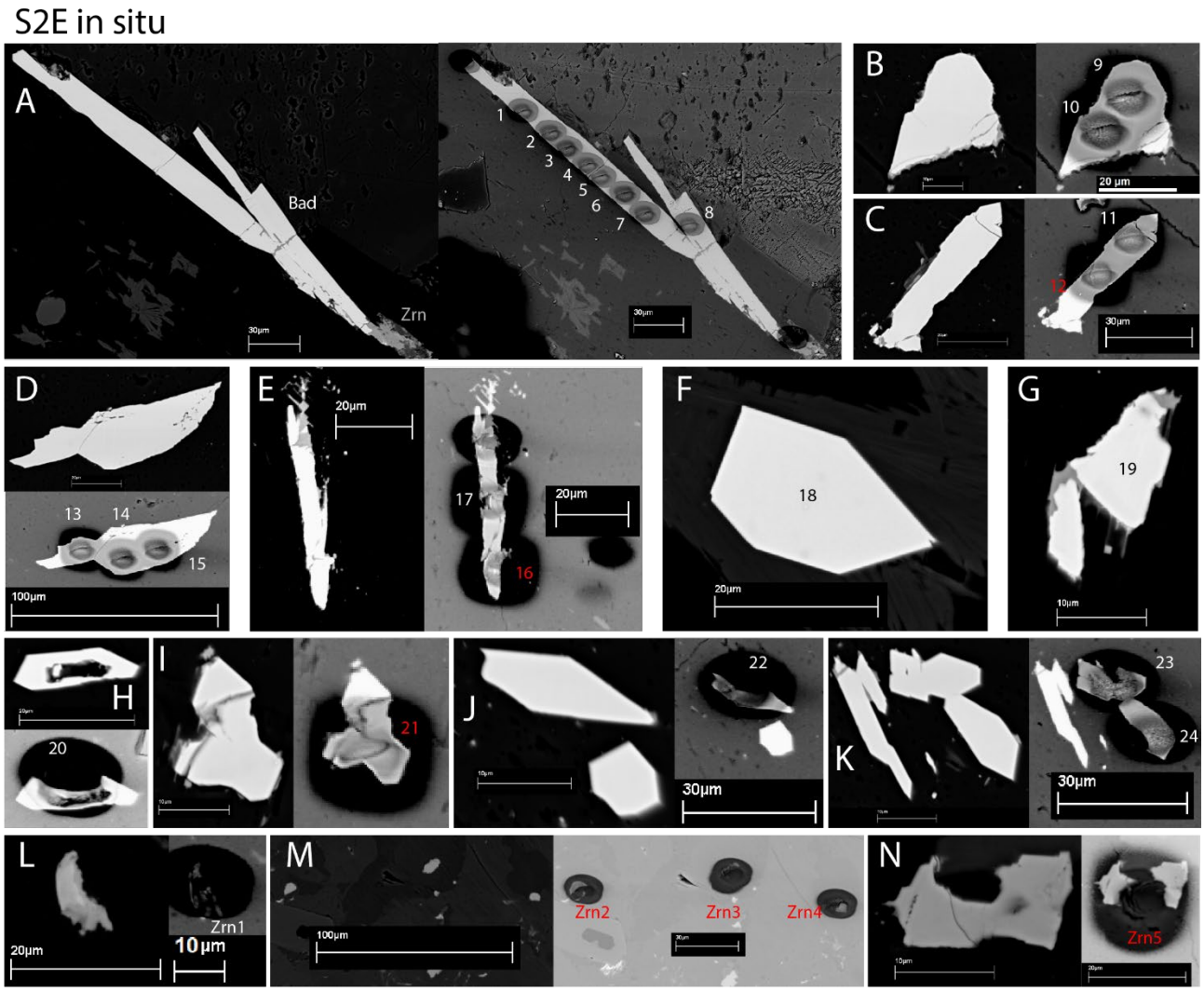

Figure S7. BSE images of analyzed crystals and SIMS analysis craters of sample S2E (in situ).

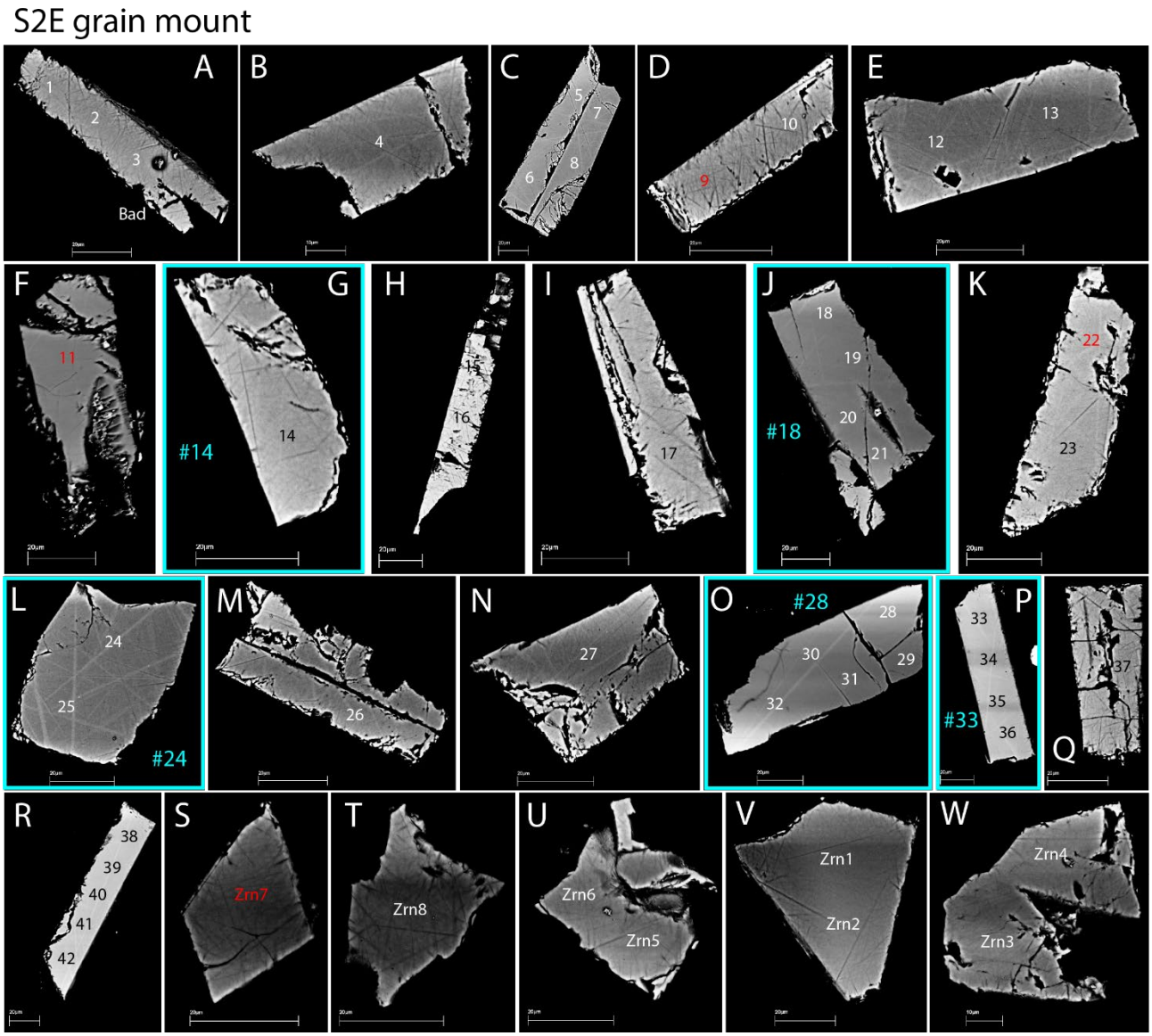

Figure S8. BSE images of analyzed crystals and SIMS analysis craters of the grain mount of sample S2E.

S2 Details of SIMS and ID-TIMS U-Pb preparation and analytical conditions

For preparing in situ mounts, baddeleyite-bearing parts of petrographic thin section were cut using a diamond saw, and mounted in a 25.4 mm epoxy disk along with pre-polished epoxy blocks of reference baddeleyite and/or zircon. Grain mounts were made when crystals detected in thin section were large enough for mineral separation (>50 µm). In this case, the rock was crushed and sieved to <200 µm. Usage of the electromagnetic Frantz separator at 1.5–2.0 A and 5–15° tilt was found inefficient, and hence abandoned. Instead, baddeleyite was concentrated via hydraulic separation in a water-filled bowl, followed by hand picking under a binocular microscope. Separated crystals were then embedded in epoxy along with reference baddeleyite and/or zircon, and sectioned using SiC paper (4000 grit) and diamond suspension (1 µm, ¼ µm).

Automated mass calibration for SIMS analysis was employed, with shifts for Pb peaks referenced to that for Zr_2O, and the Th species (Th and ThO) against U and UO_2, respectively. For analyses of reference materials and grain mount sessions, a chain of spots was run automatically, employing automated pre-sputtering and beam centering. When unknowns of in situ analyses were analyzed, automated analysis chains were not applicable, so the Z position of the sample stage had to be adjusted manually prior to each analysis, compensating slight differences in sample height. Beam centering and spot finding were executed in the same step by using the $^{180}Hf^{16}O$ secondary ion image. The $^{206}Pb/^{238}U$ age and U concentrations of the reference materials were used to calculate those of the samples. Baddeleyite, zircon and zirconolite were analyzed in multiple sessions between 10/19/2017 and 07/20/2018. All SIMS data have been evaluated using the ZIPS software (version 3.1.1).

For ID-TIMS data from S2E and FP6D, baddeleyite grains were plucked from the SIMS mount, spiked with $^{205}Pb/^{233}U/^{235}U$ tracer (ET535) and dissolved in HCl acid in teflon microcapsules. ID-TIMS measurements used single Daly-photomultiplier mode on a Micromass Sector 54 thermal ionization mass spectrometer at the University of Wyoming. Mass discrimination for Pb was 0.200 ± 0.10 %/amu for Daly analyses based on replicate analyses of NIST SRM 981. U fractionation was determined internally during each run. Measured procedural blanks averaged 0.8 pg Pb. U blanks were consistently less than 0.1 pg. Isotopic composition of the Pb blank was measured as 18.5268 ± 0.45, 15.6046 ± 0.41, and 38.0332 ± 0.73 for $^{206}Pb/^{204}Pb$, $^{207}Pb/^{204}Pb$ and $^{208}Pb/^{204}Pb$, respectively. The sample weight was estimated from grain dimensions assuming a density of 6.02 g/cm^3; U and Pb concentrations are based on these estimates. Picograms (pg) sample and common Pb are measured directly from isotope dilution measurements.

For ID-TIMS data from SL18, the grains were dissolved in concentrated HF, spiked with the EARTHTIME 202Pb-205Pb-233U-235U spike (calibration v3, Condon et al., 2015; McLean et al., 2015) and run through ion exchange column chemistry before TIMS analysis. All data were processed using both the Redux and Tripoli software utilizing the equations of McLean et al. (2011).

S3 Geochemistry - analytical conditions

All geochemical analyses were performed by geochemical laboratories of the GFZ Potsdam. Concentrations of major elements (reported in oxide wt. % with Fe as Fe_2O_3) and trace elements (Rb, Sr, Ba, Y, Zr, Nb, Zn, Cu, Ni and V) were determined by X-ray fluorescence spectrometry. Powdered samples were prepared as fused discs of Li tetraborate-metaborate (FLUXANA FX-× 65, sample-to-flux ratio 1:6) and analyzed with a PANalytical AXIOS Advanced spectrometer employing a Rh X-ray tube. H_2O and CO_2 concentrations were determined by pyrolysis with a EURO EA Element Analyzer.

Following acid dissolution of the powdered samples, further trace elements were analyzed with an ELEMENT 2XR high-resolution sector field mass spectrometer (HR-ICP-MS) using inductively coupled plasma as an ion source. The following

isotopes were used for analysis: ^{7}Li, ^{9}Be, ^{45}Sc, ^{59}Co, ^{63}Cu, ^{75}As, ^{98}Mo, ^{114}Cd, ^{118}Sn, ^{121}Sb, ^{133}Cs, ^{178}Hf, ^{205}Tl, ^{208}Pb, ^{209}Bi, ^{232}Th, ^{238}U. The values reported are the average of duplicate measurements from the same solution.

The rare-earth elements were analyzed by Inductively Coupled Plasma Optical Emission Spectrometry (ICP-OES) after a lithium metaborate-sodium perborate dissolution followed by the column purification technique. With an Agilent 5110 ICP-OES, the isotopes ^{139}La, ^{140}Ce, ^{141}Pr, ^{146}Nd, ^{149}Sm, ^{151}Eu, ^{157}Gd, ^{159}Tb, ^{163}Dy, ^{165}Ho, ^{167}Er, ^{169}Tm, ^{172}Yb, and ^{175}Lu were analyzed in high-resolution mode.

S4 SIMS results for sample S2C (zircon)

Zircon dates from S2C are largely in the similar range as those for S2E baddeleyite, but some analyses are up to 50% younger (Fig. S9; Table S4). Most analyses show high common Pb, especially those with the youngest ages. Baddeleyite inclusions in zircon were too small to analyze.

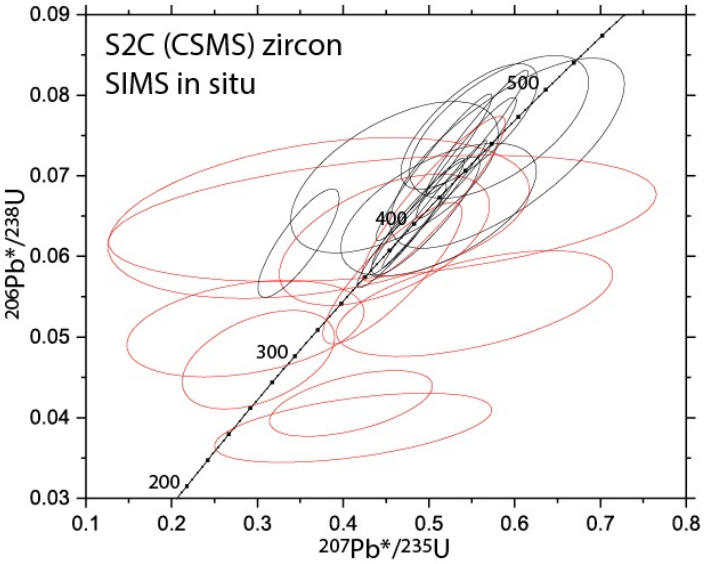

Figure S9. U-Pb results of S2C (1σ error ellipses). Analyses in red are those with the highest proportion of common Pb.

S5 Effect of choice of Pb isotopic compositions on ID-TIMS data interpretation

For analyses with common Pb quantities above blank, the choice of Pb isotopic compositions of common Pb can affect concordia coordinates, linear regressions and ^{207}Pb/^{206}Pb dates. Baddeleyite ID-TIMS data from FP6D and S2E demonstrate a direct correlation between increasing ^{207}Pb/^{206}Pb dates and discordance with corresponding negative lower intercepts when reduced with Stacey and Kramers (1975) model Pb isotopic compositions for 500 Ma (^{206}Pb/^{204}Pb, ^{207}Pb/^{204}Pb of 17.914, 15.564). To test whether this pattern was a result of the choice of isotopic compositions, we plotted ^{206}Pb/^{204}Pb vs. ^{207}Pb/^{204}Pb of total Pb and blank-corrected Pb from FP6D baddeleyite ID-TIMS analyses. Both plots have poor linear statistics (mean square weighted deviates, MSWD, of 8 and 3 respectively, with probability of fits of 0 and 2%, Figure S10), indicating that either there are variable isotopic compositions of common Pb or multiple ^{207}Pb/^{206}Pb dates, or both.

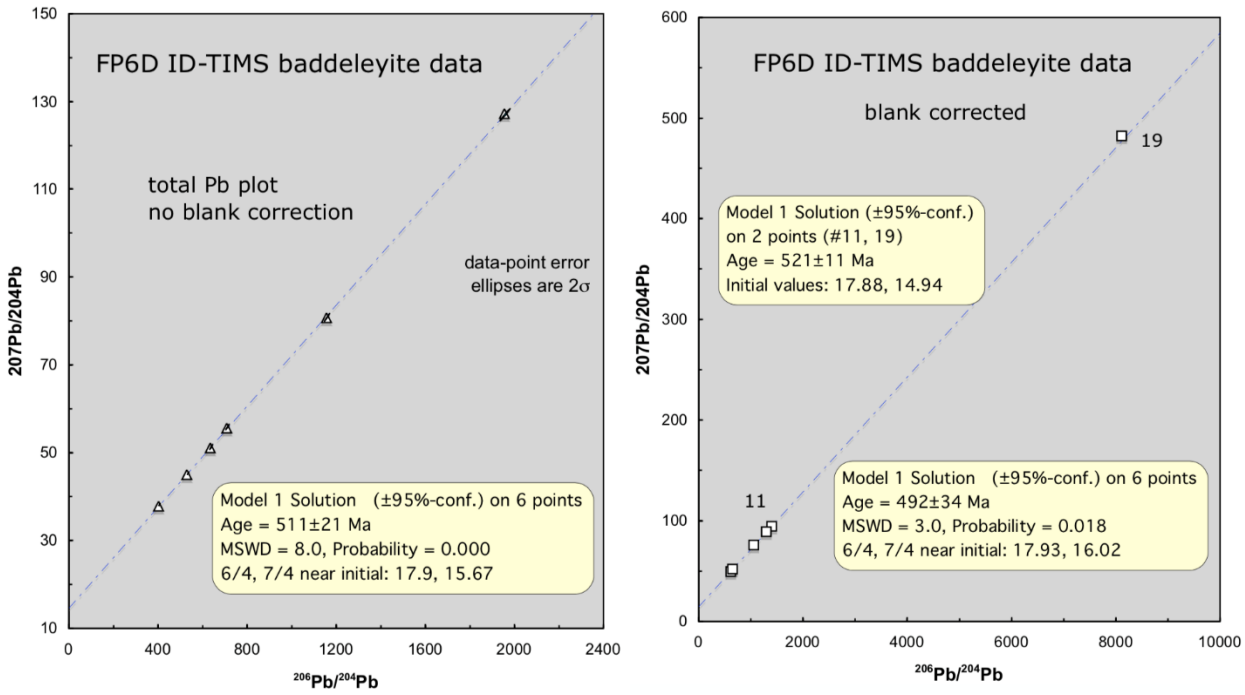

Figure S10. $^{207}Pb/^{204}Pb$ vs. $^{206}Pb/^{204}Pb$ isochron plots of total Pb data from FP6D baddeleyite analyses to test for linearity; plot on the left does not include any correction for measured Pb blank and tests whether or not all the common Pb can be ascribed to a single blank source. The poor linear fits of these data, with high MSWDs and low probabilities of fit, require either multiple sources of common Pb and/or multiple $^{207}Pb/^{206}Pb$ dates of the analyses.

As a further test, we calculated the initial Pb isotopic compositions needed to produce the same $^{207}Pb/^{206}Pb$ dates from analyses #11 and #19, the two analyses with the highest radiogenic to common Pb ratios (Pb*/Pbc in Table 3, 16.8 and 28.8). These two analyses are the least affected by the choice of initial Pb isotopic compositions, but nonetheless have $^{207}Pb/^{206}Pb$ dates that are different and outside of error (503.9±6.0 vs. 517.9±6.9 Ma) when reduced with Stacey and Kramers (1975) model values. Their two-point blank-corrected Pb-Pb isochron solution is 521±11 Ma with initial Pb isotopic compositions of 17.88 and 14.94 ($^{206}Pb/^{204}Pb$, $^{207}Pb/^{204}Pb$ calculated at Stacey and Kramers model value for $^{206}Pb/^{204}Pb$ at 521 Ma). These initial values are just one possible solution of a set of values that lay along the Pb-Pb isochron. This set of initial Pb solutions plot well below Zartman and Doe (1980) model curves for various Earth reservoirs (Figure S11), in a region of Pb-Pb space that is not geologically reasonable. Furthermore, the Pb isotopic values that are required to produce Pb-Pb dates of 521 Ma from each of the other 4 analyses are widely divergent with $^{207}Pb/^{204}Pb$ values that range from 15.90 to 15.45 at $^{206}Pb/^{204}Pb$ of 17.88 (Figure S11). In summary, there is no single Pb isotopic composition that will produce overlapping $^{207}Pb/^{206}Pb$ dates from all the baddeleyite analyses from FP6D.

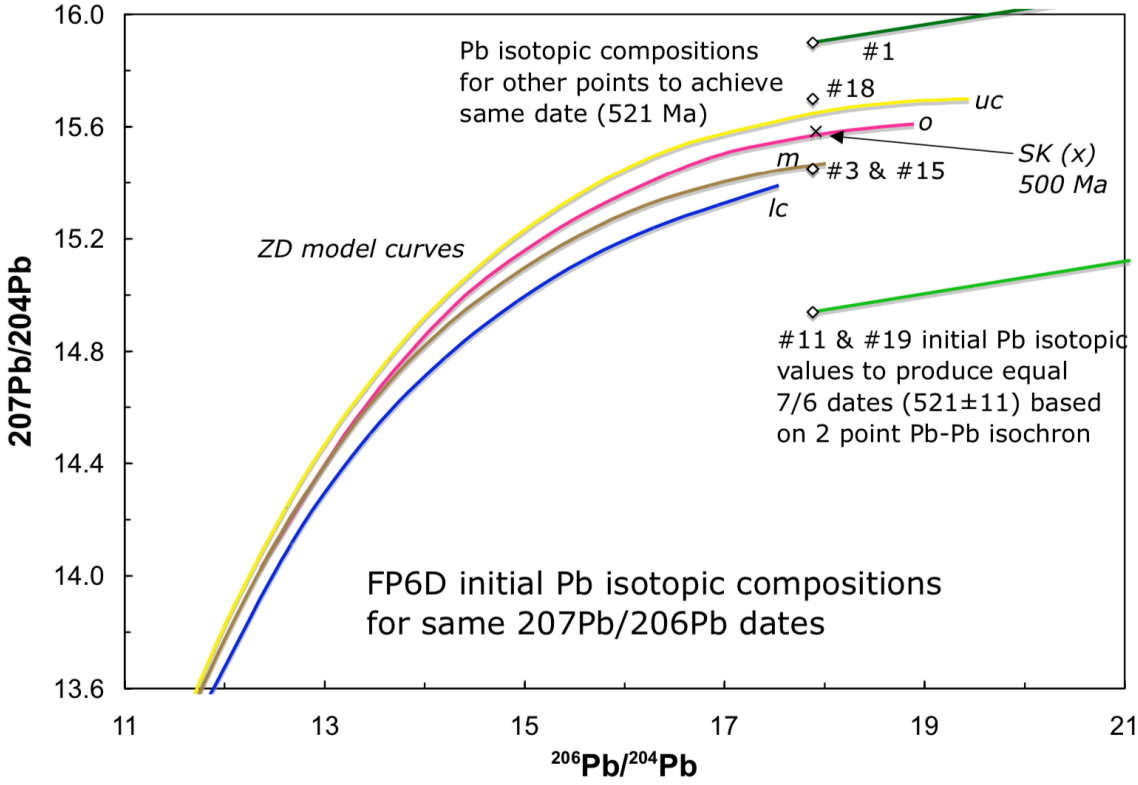

Figure S11. $^{207}Pb/^{204}Pb$ vs. $^{206}Pb/^{204}Pb$ plot of initial Pb isotopic solutions needed to produce overlapping $^{207}Pb/^{206}Pb$ dates from the baddeleyite analyses of FP6D. Isotopic solutions form lines (green) with 521 Ma slopes; diamonds indicate the solution values corresponding to $^{206}Pb/^{204}Pb$ of 17.88. Zartman and Doe (1980) model curves and Stacey and Kramers (1975) model values for 500 Ma are shown for comparison. Isotopic values needed to converge the Pb-Pb dates from baddeleyite #11 and #19 are not reasonable geologically; the wide range of values needed to resolve the other dates to 521 Ma requires grain-by-grain variation in initial Pb, which is untenable. uc = upper crust, o = orogene, m = mantle, lc = lower crust.

To demonstrate the effect of various choices of initial Pb isotopic composition on concordia regressions, we also plotted FP6D baddeleyite data reduced with three potential model compositions at ca. 500 Ma, Zartman and Doe (1980) mantle and upper crust and Stacey and Kramers (1975) (Figure S12). Data from analyses #11 and #19 are the most robust regarding these different reductions, consistent with their high radiogenic to common Pb ratios (Pb*/Pbc). Regressions of data reduced with Zartman and Doe (1980) upper crust and Stacey and Kramers (1975) Pb isotopic values both have good linear fits with MSWDs of 1.6 and 1.7 and probabilities of fit of 18 and 15%, respectively. They produce overlapping upper intercept dates ca. 498 Ma, but negative lower intercepts outside of error (-479 Ma). Data reduced with Zartman and Doe (1980) model mantle values have significant scatter, with much poorer linear statistics (MSWD of 2.4, probability of fit of 4.5%). The lower intercept from mantle-reduced data has a negative mean (-458 Ma) although it overlaps zero within error due to the high variation in slope from the high scatter. We favor interpretations based on the best linearity of data (Stacey and Kramers or Zartman and Doe upper crust), as these include all the baddeleyite analyses and indicate the simplest U-Pb systematics. The correlation of increasing $^{207}Pb/^{206}Pb$ dates with increasing discordance (and associated negative lower intercepts) requires an additional discordance mechanism besides recent bulk Pb loss. Excess ^{207}Pb from the decay of ^{231}Pa can produce $^{207}Pb/^{206}Pb$ dates that are too old, but the effect should be relatively consistent for each baddeleyite grain and would not produce the observed correlation with discordance. Deficit of ^{206}Pb from ^{222}Rn escape would also produce $^{207}Pb/^{206}Pb$ dates that are too old and could more easily correlate with bulk Pb loss discordance as both mechanisms involve element loss out of the baddeleyite crystals.

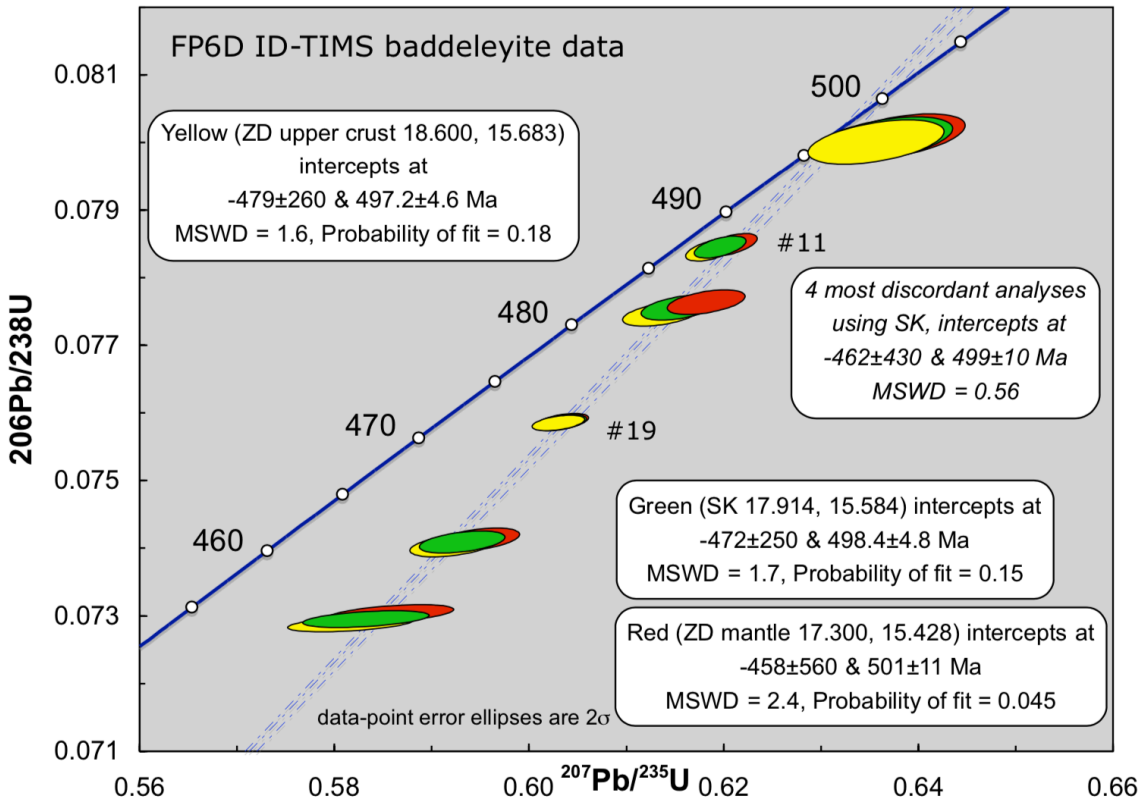

Figure S12. Concordia plot of baddeleyite data from FP6D using various model reservoirs for common Pb corrections. Zartman and Doe (1980) mantle values produce an array with poor linear statistics and is not favored. Reductions using either Zartman and Doe (1980) upper crust or Stacey and Kramers (1975) model values lead to regressions with good linear statistics (MSWD 1.6 to 1.5, probability of fits of 15 to 18%). A regression limited to the four most discordant analyses also produces a negative lower intercept (-462±430 Ma), which demonstrates that the negative lower intercept is related to discordance and is not an artifact due to variation between the two least discordant analyses.

S6 Duluth gabbro evidence for isotopically-biased discordance in baddeleyite.

Recent studies of coexisting zircon and baddeleyite from the ca. 1.1 Ga Duluth gabbro complex demonstrate that discordance in baddeleyite may require isotopically-biased mechanisms in addition to bulk Pb loss (Hoaglund, 2010; Ibañez-Mejia and Tissot, 2019). In those studies, ID-TIMS baddeleyite data produced older $^{207}Pb/^{206}Pb$ dates than chemically-abraded (CA) ID-TIMS zircon data (Figure S13). Assuming that the CA-ID-TIMS zircon dates reflect the time of baddeleyite crystallization, either excess ^{207}Pb due to the decay of ^{231}Pa followed by varying degrees of recent bulk Pb loss, or a deficit of ^{206}Pb due to ^{222}Rn escape are required to explain the data arrays (Figure S13). ^{206}Pb loss alone can explain many of the baddeleyite analyses as the $^{207}Pb/^{235}U$ dates of the least discordant baddeleyite analyses overlap with the zircon $^{207}Pb/^{235}U$ dates, but minor recent bulk Pb loss is also required to explain the more discordant baddeleyite. The magnitude of recent bulk Pb loss is significantly higher for the ^{207}Pb excess mechanism than for the ^{206}Pb deficit one for these data. The baddeleyite data array may reflect operation of all three mechanisms to varying degrees as well. In light of our evidence for correlation between isotopic bias and discordance from FP6D, we interpret the Duluth data to reflect a strong component of preferential ^{206}Pb loss.

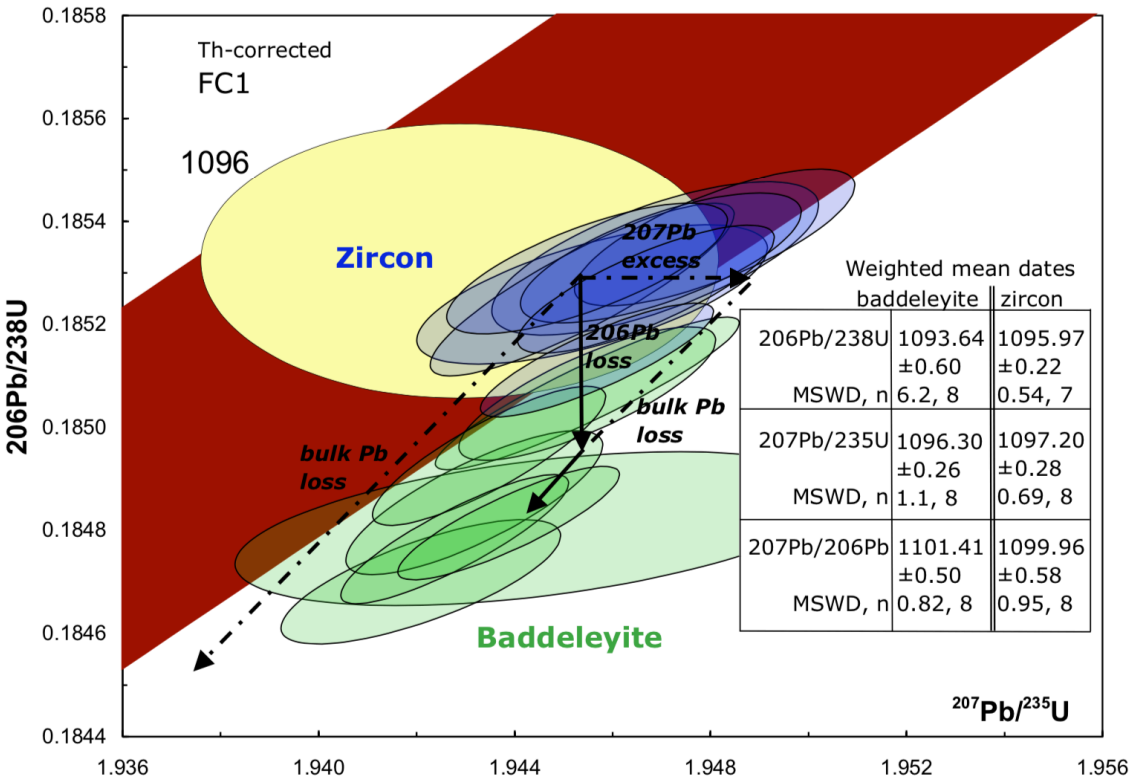

Figure S13. Concordia plot of data from Ibañez-Mejia and Tissot (2019) of coexisting zircon (CA-ID-TIMS) and baddeleyite (ID-TIMS) from Duluth Gabbro sample FC-1. Discordance mechanisms to explain the baddeleyite array are shown by arrows. Bulk Pb loss trajectories assume recent Pb loss.

S7 Results of whole-rock geochemistry

Results for major and trace elements (Table S7; Fig. S14-S16) are in good agreement with the data of Greenough (1984), except the rare earth elements, which he analyzed by X-ray fluorescence.

Supplementary references:

Condon, D. J., Schoene, B., McLean, N. M., Bowring, S. A., and Parrish, R. R.: Metrology and traceability of U–Pb isotope dilution geochronology (EARTHTIME Tracer Calibration Part I). Geochim. Cosmochim. Acta, 164, 464–480, 2015.

McLean, N. M., Bowring, J. F., and Bowring, S. A. An algorithm for U-Pb isotope dilution data reduction and uncertainty propagation. Geochem. Geophys. Geosyst., 12, Q0AA18, 2011.

McLean, N. M., Condon, D. J., Schoene, B., and Bowring, S. A. Evaluating uncertainties in the calibration of isotopic reference materials and multielement isotopic tracers (EARTHTIME Tracer Calibration Part II). Geochim. Cosmochim. Acta, 164, 481–501, 2015.

Sun, S.-s. and McDonough, W. F.: Chemical and isotopic systematics of oceanic basalts: implications for mantle composition and processes. Geological Society, London, Special Publications, 42(1), 313–345, 1989.

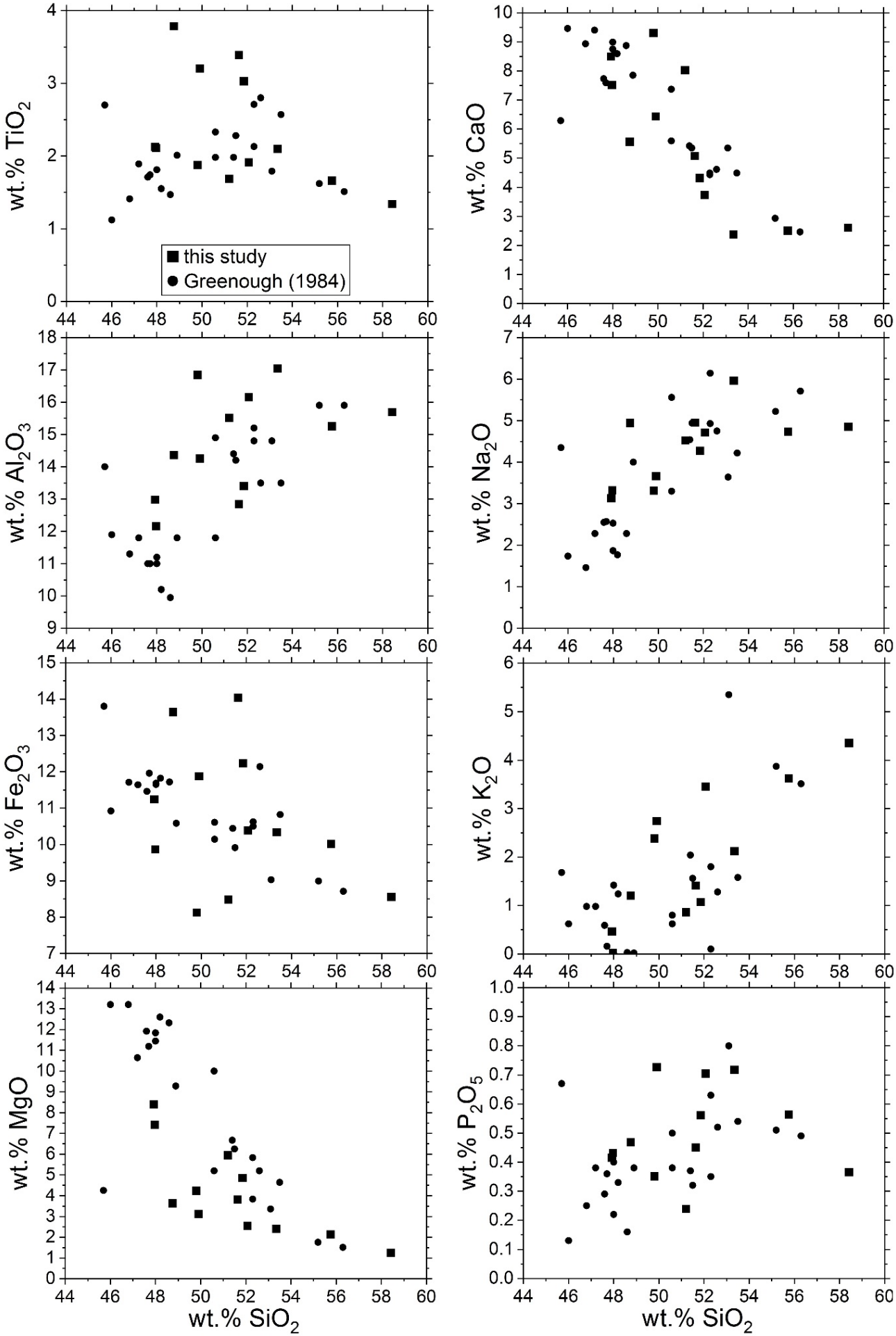

Figure S14. Major element contents of rocks from the Spread Eagle Intrusive Complex.

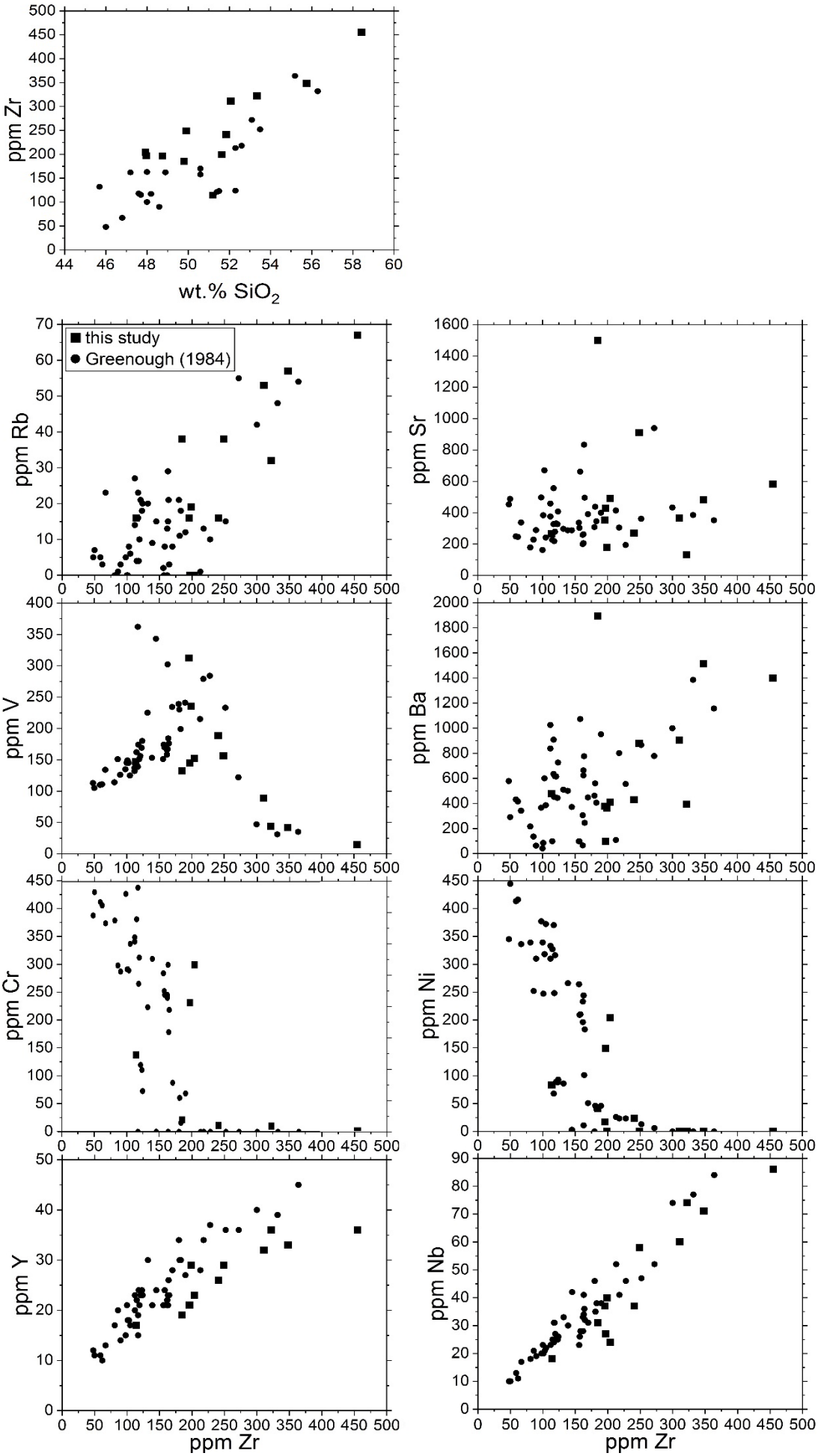

Figure S15. Trace element contents of rocks from the Spread Eagle Intrusive Complex.

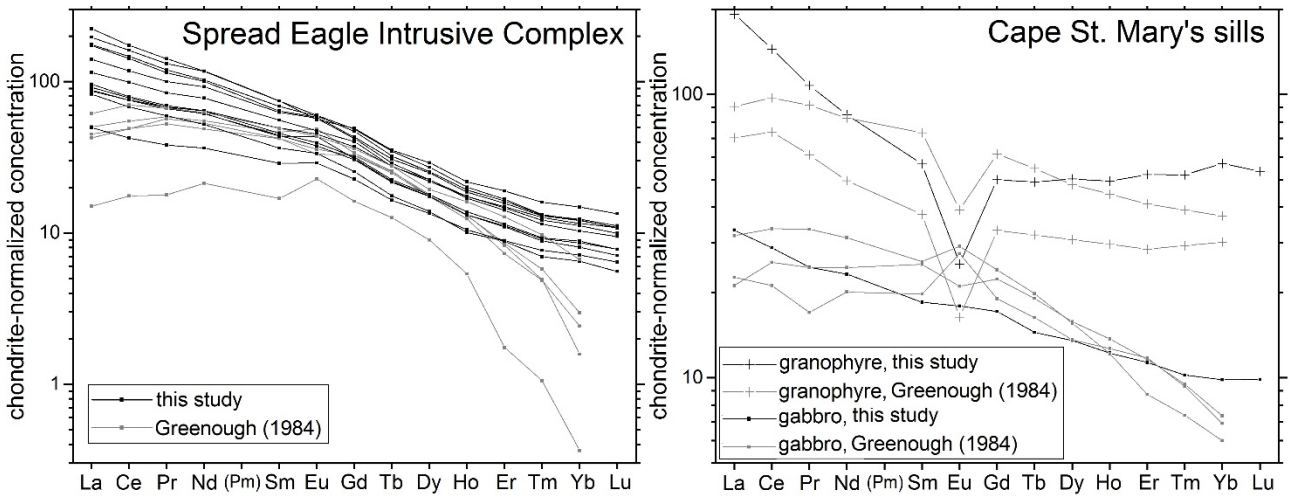

Figure S16. Rare earth element contents of rocks from the Spread Eagle Intrusive Complex and Cape St. Mary's sills, normalized to chondritic values after Sun and McDonough (1989). Note that the analyses of Greenough (1984) were done by X-ray fluorescence spectrometry, whereas ICP-OES was employed in our study.